THE JOURNAL OF PHYSICAL CHEMISTRY LETTERS
A JOURNAL OF THE AMERICAN CHEMICAL SOCIETY

pubs.acs.org/JPCL Letter

Predicting Spontaneous Orientational Self-Assembly: *In Silico* Design of Materials with Quantum Mechanically Derived Force Fields

Giacomo Prampolini,* Leandro Greff da Silveira, J. G. Vilhena, and Paolo Roberto Livotto

Cite This: https://doi.org/10.1021/acs.jpclett.1c03517 Read Online

ACCESS | Metrics & More | Article Recommendations | Supporting Information

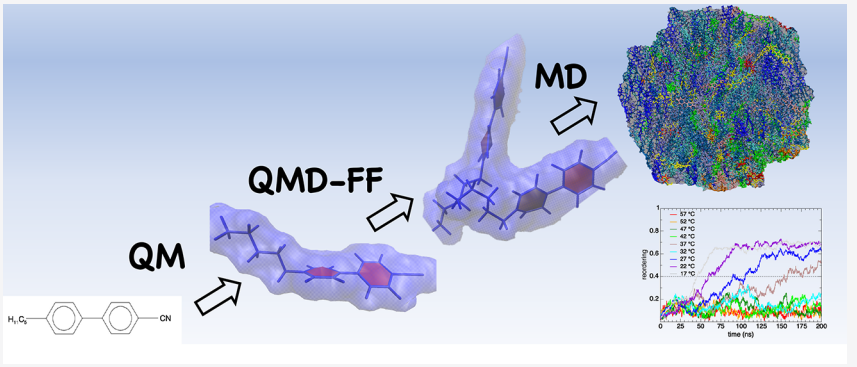

ABSTRACT: *De novo* design of self-assembled materials hinges upon our ability to relate macroscopic properties to individual building blocks, thus characterizing in such supramolecular architectures a wide range of observables at varied time/length scales. This work demonstrates that quantum mechanical derived force fields (QMD-FFs) do satisfy this requisite and, most importantly, do so in a predictive manner. To this end, a specific FF, built solely based on the knowledge of the target molecular structure, is employed to reproduce the spontaneous transition to an ordered liquid crystal phase. The simulations deliver a multiscale portrait of such self-assembly processes, where conformational changes within the individual building blocks are intertwined with a 200 ns ensemble reorganization. The extensive characterization provided not only is in quantitative agreement with the experiment but also connects the time/length scales at which it was performed. Realizing QMD-FF predictive power and unmatched accuracy stands as an important leap forward for the bottom-up design of advanced supramolecular materials.

Spontaneous emergence of highly ordered molecular architectures, a process known as supra-molecular self-assembly, is a matter of utmost practical and fundamental interest.[1−8] The practical interest is best realized by its ubiquity in both biology[6] (*e.g.*, regulation of protein folding[9] and cell−cell interactions[10]) and in current and emerging technologies (*e.g.*, liquid crystal displays,[11] CO_2 capturing nanoarchitectures,[12] next-generation lithography,[13] and up to artificial molecular machines[14]). The spontaneous assembly is often activated by thermal fluctuations, which are then steered by noncovalent intermolecular interactions (*e.g.*, electrostatic and van der Waals) that direct individual building blocks to assemble into supramolecular structures endowed with novel functionalities and properties.[3,8,11,15] Therefore, molecular self-assembly could, in principle, be engineered/predicted from the chemical nature of the individual building blocks.[4,8,10,13] However, this is not generally the case,[8,10] and *de novo* design of programmed self-assembly or relating molecular structure to meso/macro-scale properties is thus a matter of vibrant research.[3,10,15−17] One of the major obstacles of this endeavor is understanding the role of single-molecule conformational flexibility,[10] which often leads to complex and shallow free energy surfaces, where the dynamics is governed by a delicate balance between entropic and enthalpic terms in an intrinsically multiscale process.[8] Over the past decades, experiments have excelled in providing an increasingly detailed picture of the nature and dynamics of intermolecular interactions governing molecular self-assembly. Despite their undisputed success, experiments have several limitations, including the following: (i) No single experiment provides a multiscale description (picosecond/picometer vibrations of individual building blocks up to millisecond/millimeter molecular assemblies); thus, an often unpractical combination of many

Received: October 27, 2021
Accepted: December 10, 2021

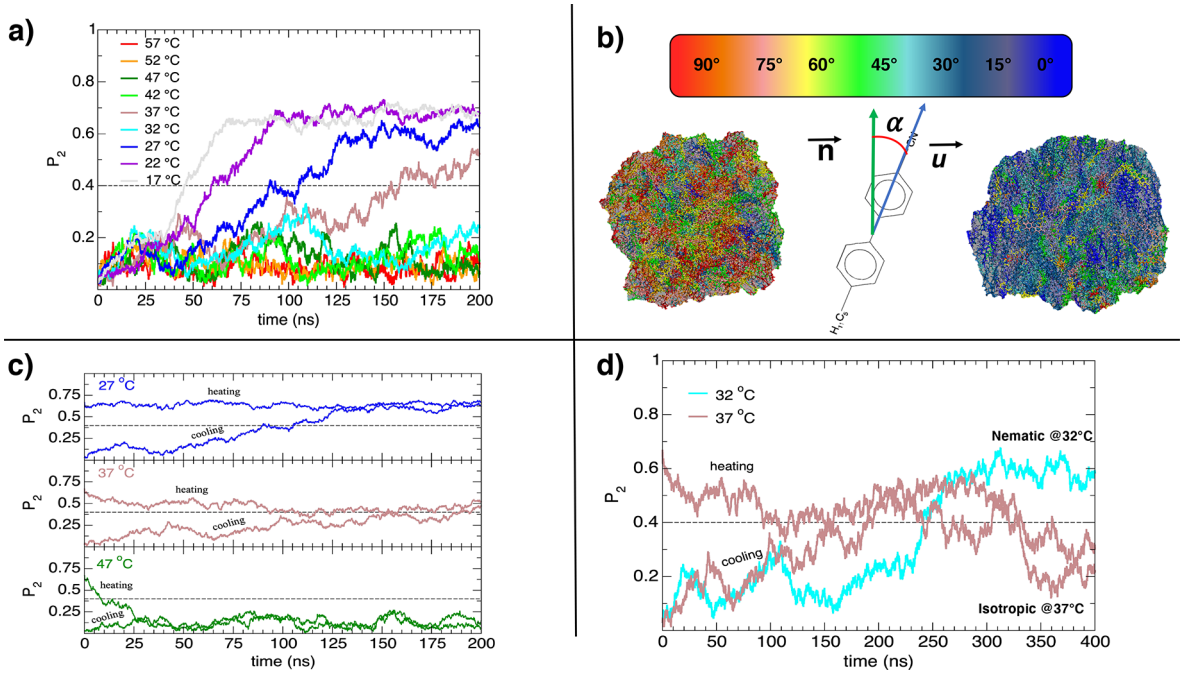

Figure 1. Spontaneous self-assembly onto ordered supramolecular structures upon cooling. (a) Computed order parameter (P_2) vs time, upon cooling at different temperatures in the 17−57 °C range; (b) final isotropic (left) and nematic (right) configurations. The color code highlights the degree of orientation of each molecule along the phase director $\hat{\mathbf{n}}$; (c) P_2 convergence of the cooling/heating sequences at 27 °C (blue), 37 °C (brown), and 47 °C (green); (d) P_2 long time convergence at 32 °C (cyan) and 37 °C (brown), near the experimental T_{NI} (33.7 °C[49]).

experiments is required. (ii) Most techniques measure ensemble averages,[8,10,18] from which follows our scarce understanding of pivotal single-molecule trigger events such as nucleation. These limitations have severely hampered our ability to relate chemical structure to thermodynamic properties of the ensemble, especially if the composing building blocks are small flexible molecules. In this framework, theoretical approaches offer an invaluable tool to bridge the gap, as they provide an atomically detailed picture of the self-assembly of large complex molecules with unmatched temporal resolution (from ps to ms).[10,18]

All-atom molecular dynamics (MD) is arguably one of the most widely used methods to unveil dynamic or non-equilibrium atomic processes at the nanoscale.[19,20] Its reliability hangs, however, on the accuracy of the adopted interatomic potentials, also known as force fields (FFs).[21] Although the structure and dynamics of large biomolecules are often well accounted for by general-purpose transferable FFs,[22] this is not true for other supra-molecular materials, where a partial refinement or a complete reparameterization is required.[23−27] A sound and elegant route to meet this is to resort to quantum mechanical (QM) calculations to derive the FF parameters based on a higher-level QM description.[28] Such strategy brings in three advantages of utmost relevance to supramolecular chemistry: (a) predictive power (an attribute endowed by the *first-principles* nature of the sourcing QM simulations); (b) high accuracy and chemical-specificity (at variance with transferable FFs, QM-derived FFs (QMD-FFs) are custom-made and thus are capable of capturing the chemical specificity of each molecule); and (c) reliability at varied thermodynamic conditions (because QM parametrization reproduces a thermodynamic independent potential energy surface, at variance with empirical parametrization schemes that are usually limited to specific thermodynamic conditions). Such attributes position QMD-FFs as a method of choice to rationalize specific structure−property relationships, accurately predict the macroscopic behavior of supra-molecular assemblies, stimulate new experiments, and eventually bring us closer to a *de novo* design of programmed assembly based on solely the molecular structure. Unfortunately, fulfilling such potential has remained an elusive task.[29−31] In particular, large-scale supra-molecular reorganization processes, where single-molecule events are intertwined with slow (>100 ns), thermally driven collective dynamics have never been investigated with QMD-FFs. In fact, even in the most recent applications reported in the literature, the observation time was limited to few nanoseconds of simulation.[29,30]

In this work, we show that QMD-FF provides a truly multiscale description of the complex self-assembly process that leads to an orientationally ordered phase upon cooling in ambient conditions with a remarkable accuracy and, to the best of our knowledge, the first atomically detailed picture of a self-reorganization processes spanning over 200 ns. To this end, we adopt a specific and accurate QMD-FF, recently[31] parametrized according to the Joyce/Picky procedure,[32−35] for the 4′-*n*-pentyl-4-cyanobiphenyl (5CB), a well-known benchmark liquid-crystalline molecule. The results recently achieved therein suggested that the dramatic failure of general-purpose FFs, which predict a spontaneous assembly at temperatures more than 120 °C higher than the experiment,[31,36] could be significantly corrected by QMD-FFs. Yet, despite the promise, the MD outcomes reported in ref 31 did not allow for a detailed characterization of the supramolecular architecture or for an atomistic insight into the processes possibly leading to the orientational reorganization, thus calling for a further, more extended investigation. Liquid crystals (LCs) are indeed the ideal candidate to test QMD-FFs reliability for self-assembled materials. On the one hand, the natural predisposition of LCs to self-organize into ordered supramolecular structures[37] has been exploited by recent research to set up a large variety of

https://doi.org/10.1021/acs.jpclett.1c03517
J. Phys. Chem. Lett. XXXX, XXX, XXX−XXX

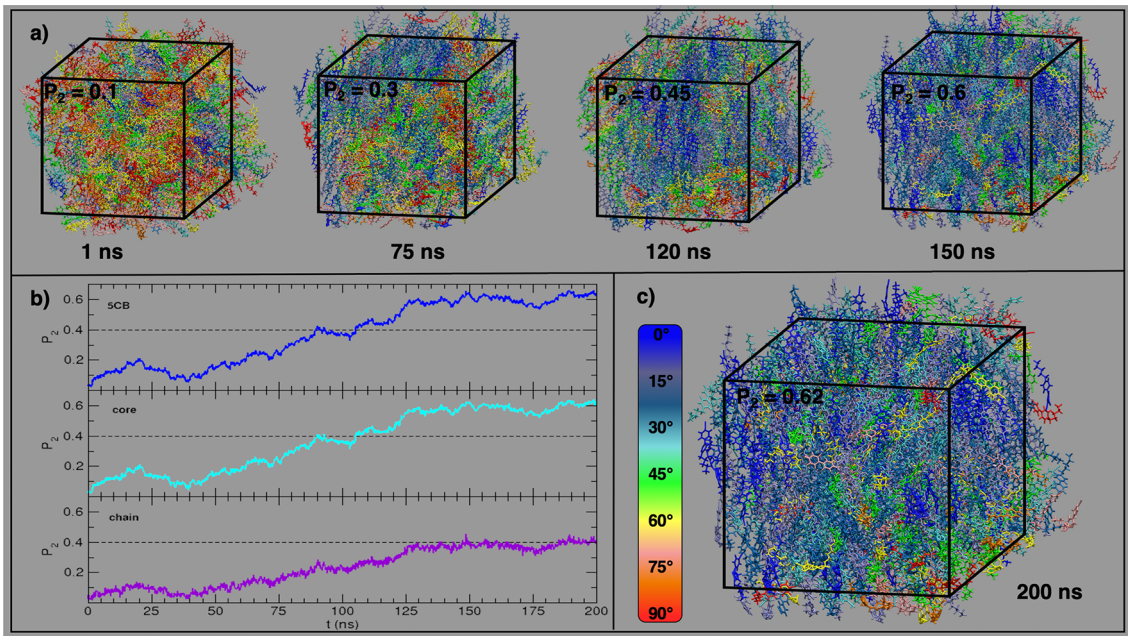

Figure 2. Spontaneous self-ordering at room temperature (27 °C) and 1 atm. (a) Pictorial view of the reorienting process during the first 150 ns, see Figure 1 for color code; (b) orientational order parameter P_2 vs time computed for the whole molecule (top panel, blue line), for the CB core (middle panel, cyan line), and for the aliphatic chain (bottom panel, violet line); (c) final equilibrated configuration at 27 °C.

advanced materials.[11,13,38−41] On the other hand, among other soft assemblies, LCs are indeed a challenging benchmark for any *in silico* approach with predictive aims, because (i) the molecular detail profoundly influences both the structure and thermodynamic macroscopic properties of the material[37] and (ii) the complex reorientational dynamics that leads to the ordered supramolecular structure takes place over significantly different time scales.[11,13,41] Furthermore, the wealth of experiments[42−58] characterizing both the different stages of the thermally driven orientational reorganization and the resulting isotropic and nematic phase makes 5CB a perfect benchmark.

Two separate series of MD runs (*i.e.*, a heating sequence from an orientationally ordered configuration and a cooling one from the isotropic liquid) were devised to determine the 5CB nematic to isotropic (T_{NI}) transition temperature. These calculations were carried out using GROMACS,[59] on a system composed of 1000 molecules (further details are provided in the Supporting Information). In Figure 1a the order parameter P_2 is monitored for 200 ns at each temperature explored in the cooling sequence.

A spontaneous self-assembly into an orientationally ordered structure clearly appears at the lower temperatures. The reordering process at 27 °C takes place in about 100 ns, leading the system from a completely disordered phase, shown in the left part of Figure 1b, into a nematic ordered phase, displayed on the right. The mechanical equilibrium and stability of the final bulk condensed phases are confirmed in Figure 1c, where the convergence of the order parameter is apparent at all temperatures, and are shown to be independent from the starting configuration (isotropic or orientationally ordered in the cooling and heating sequence, respectively). Note that the spontaneous reordering time noticeably increases as temperature rises from 17 to 37 °C. It could be thus inferred that 200 ns is not enough to equilibrate the system near the phase transition temperature. Indeed, Figure 1d shows the P_2 convergence at 32 and 37 °C when the *NPT* runs are extended to 400 ns: the two equilibrated configurations do invert their ordering, with the low temperature one being nematic and the other being isotropic. Noticeably, based on these findings, the transition temperature for the spontaneous transition could be placed at 34.5 ± 2.5 °C, well within the experimental T_{NI} (33.7[49] to 35.2[55] °C).

This remarkable agreement prompted us to confidently exploit the unique possibility offered by MD simulations to go across different time and length scales and thus to further investigate the self-assembly process at an atomistic/molecular scale. Figure 2a shows an atomically detailed view of the supramolecular organization upon cooling at 27 °C, where the spontaneous reordering occurring between 75 and 120 ns is displayed using a color code highlighting all molecules aligned along a preferential direction (the phase director **n**; see Figure 1b and the Supporting Information).

The progressive molecular alignment, shown Figure S3 and leading to the orientationally ordered nematic phase, can be further decomposed in terms of two 5CB building blocks, namely, the rather rigid biphenyl core and the flexible pentyl chain. The partial order parameters (P_2^{core} and P_2^{chain}; see the Supporting Information) referred to the above-mentioned moieties are displayed in Figure 2b for the 27 °C run. As detailed in Figures S4−S6, the self-assembly reorienting process does not take place continuously, but it rather proceeds in two time-separated steps: between 75 and 90 ns and between 103 and 115 ns. This is also apparent in Figure 2b, as the main contribution to the overall order parameter P_2 is given by the rigid core moiety, in particular in the second time interval. However, as indicated by the P_2^{chain} order parameter, the alignment of the flexible chains also contributes to the self-assembly process. The atomistic detail provided by our MD simulations allows gaining a deeper insight onto the mechanisms of this chain contribution. As displayed in Figures S4−S6, the P_2^{chain} increase can be traced back to a chain elongation, in turn driven by *trans−gauche* conformational changes within the aliphatic chains. This picture is confirmed

https://doi.org/10.1021/acs.jpclett.1c03517
J. Phys. Chem. Lett. XXXX, XXX, XXX−XXX

Table 1. Distributions of the Most Populated Chain Conformations in the Nematic (22 °C) and Isotropic (47 °C) Phase, Obtained by Applying Either the ELS[42,52] or a Mean-Field (MF) Model[48] to Experimentally Measured NMR Data, or in the Present Work, Analyzing the MD Trajectories

	ELS[42,52]							
	quadrupolar splittings (^{2}H)				dipolar coupling (^{13}C and ^{1}H)			
conf	ttt (%)	gtt (%)	tgt (%)	ttg (%)	ttt (%)	gtt (%)	tgt (%)	ttg (%)
nematic	33.2	9.7	23.2	14.3	32.9	9.8	20.2	14.8
isotropic	22.7	16.7	16.7	16.7	24.2	13.0	14.8	16.1
Δ_{conf}	10.5	−7.0	6.5	−2.4	8.7	−3.2	5.4	−1.3

	MF[48]			
conf	ttt (%)	gtt (%)	tgt (%)	ttg (%)
nematic	32.3	12.2	26.8	12.9
isotropic	24.6	22.0	15.8	15.0
Δ_{conf}	7.7	−9.8	11.0	−2.1

	This Work			
conf	ttt (%)	gtt (%)	tgt (%)	ttg (%)
nematic	57.0	7.6	17.5	10.3
isotropic	41.9	14.3	15.8	13.9
Δ_{conf}	15.1	−6.7	1.7	−3.6

by comparing, in Table 1, the variation Δ_{conf} of the average chain conformational population achieved in the present simulations with respect to that obtained with different NMR-based experimental techniques.[42,48,52]

It might be worth noticing that all ELS[42,52] and MF[48] values reported in Table 1 were not obtained from direct measurements but rather were extrapolated from NMR data by applying approximated statistical models, which might be the cause of the only qualitative agreement with the estimates computed in the present work. However, in going from the isotropic to the ordered nematic phase, both computed and experimental data agree in indicating a net increase of Δ_{conf} for the *ttt* population, which coincides with the most elongated shape (all-*trans* conformer, see Figure S2) of the flexible aliphatic moiety.

To further ascertain the reliability of the QMD-FF description of the spontaneous self-assembly, it is desirable to verify if the same degree of accuracy achieved at the atomistic level can be obtained when considering macroscopic observables which involve the whole bulk phase, as those characterizing the thermodynamic behavior of the LC material. Indeed, a quantitative prediction of properties such as the bulk density, transition temperature, expansion coefficient, *etc.* would be of the utmost importance if QMD-FFs have to be employed in screening protocols for *in silico* material design. Table 2 reports a detailed comparison between the bulk density, ρ, and the order parameter, P_2, achieved in simulation with their experimental counterparts.

As far as ρ is concerned, the significant density overestimation that affected our previous parametrization strategies[54,60−63] appears to be corrected by the improved accuracy of the present QMD-FF, and in particular for the nematic phase, the agreement achieved with respect to experimental data is excellent. Similarly, the vicinity of the computed P_2 to the values obtained through different experimental techniques[46,51] supports the reliability of the QMD-FF description of the self-assembling process toward an orientationally ordered phase.

Figure 3 shows the temperature dependence of two key structural and energetic descriptors, namely, the orientational order parameter (P_2, top panel) and the system enthalpy (H, bottom panel), and of their derivatives (insets).

Table 2. Computed and Experimental Density and Order Parameter at Different Temperatures in the 17−57 °C Range

	ρ (kg/m^3)		P_2	
T (°C)	comp.	exp.[53,55]	comp.	exp.[46,51]
17	1025 ± 2	1027.5−1030.1	0.69 ± 0.01	0.60
22	1021 ± 2	1022.9−1027.7	0.68 ± 0.02	0.57−0.63
27	1015 ± 2	1018.3−1021.2	0.60 ± 0.03	0.53−0.58
32	1010 ± 3	1013.7−1016.3	0.58 ± 0.04	0.44−0.50
37	1000 ± 2	1009.1−1008.1	0.25 ± 0.06	0.0
42	995 ± 3	1001.7−1004.1	0.16 ± 0.04	0.0
47	990 ± 2	997.5−999.7	0.09 ± 0.03	0.0
52	986 ± 3	993.6−996.2	0.09 ± 0.03	0.0
57	981 ± 3	989.7−992.4	0.09 ± 0.03	0.0

The phase transition temperature T_{NI} can also be determined from the latter, by locating the position of the transition peak. From the comparison of the two panels of Figure 3 it appears that both descriptors consistently agree in indicating a T_{NI} of 34.5 °C, *i.e.*, in quantitative agreement with the experiment,[49,55] as reported in Table 3.

The same table shows that a similar accuracy is achieved by MD simulations in predicting other macroscopic experimental observables often employed to describe the LC material and its transition. The nematic-to-isotropic transition enthalpy (ΔH_{NI}) and density ($\Delta\rho_{NI}$), determined by computing the difference at T_{NI} of the two regression lines shown in Figures 3 and S7, respectively, result again in values very close to the experimental range.[53,55,57,58] Similarly, the value measured[47] for the thermal expansion coefficient is within the error of α_{iso}, computed as described in Figure S8 in the Supporting Information.

After investigating the collective reorientational motion, lasting 100 ns, and having characterized the thermodynamic properties of the two resulting phases, the slow spontaneous self-assembly process can be further disentangled over different time scales to retrieve information on the single-molecule

https://doi.org/10.1021/acs.jpclett.1c03517
J. Phys. Chem. Lett. XXXX, XXX, XXX−XXX

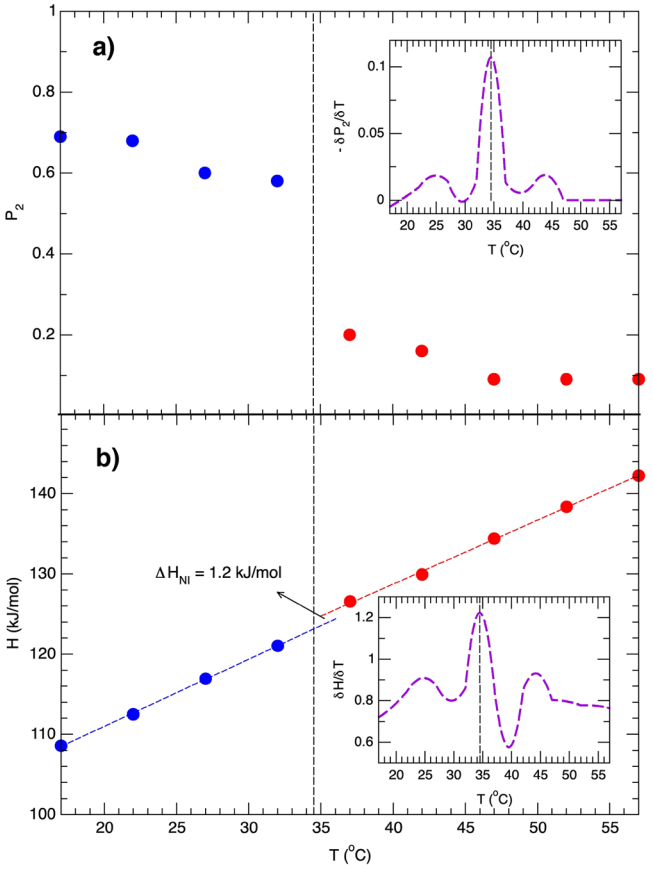

Figure 3. Phase diagrams obtained for the MD production runs at 1 atm in the 17−57 °C range. In both panels the computed properties corresponding either to a nematic or an isotropic phase are displayed with blue and red circles, respectively. (a) P_2 vs T; in the inset, the transition peak of the order parameter derivative with respect to temperature is displayed with a violet line. (b) Enthalpy vs T; linear regression fits are shown with dashed lines, whereas in the inset, the transition peak of the enthalpy derivative with respect to temperature is displayed with a violet line.

Table 3. Computed and Experimental Thermodynamic Characterization: Thermodynamic Properties at the Transition (T_{NI}, ΔH_{NI}, α_{iso}) and Reorientational Properties of the LC Material (ΔE^{a}_{transl} and γ_1)

property	this work	exp. [ref]
T_{NI} (°C)	34.5 ± 2.5	33.7−35.2 [49, 55]
ΔH_{NI} (kJ/mol)	1.2 ± 0.3	0.48−0.73 [57, 58]
$\Delta\rho_{NI}$ (kg/m^3)	4.6 ± 1.5	2.8−4.5 [53, 55]
α_{iso} (10^{-3}K^{-1})	1.0 ± 0.3	0.7 [47]

dynamics, both in medium (1−10 ns) and fast (<10 ps) time regimes. The top two panels of Figure 4 show the temperature dependence of the computed translational (D^{tr}, top) and rotational (D^{rot}, middle) diffusion coefficients (see the Supporting Information for further details) and compares them to the available experimental data. The translation of the 5CB molecules is well-described, and the experimental and computed coefficients are in very good agreement along the whole range of explored temperatures. Moreover, as already observed for the bulk density, it is worth mentioning that the present QMD-FF also overcomes the main drawback of our older models,[60,61] *i.e.*, a severe overestimation of the translational diffusion coefficient by a factor larger than 4.[54,61,62] Nonetheless, in agreement with the experiment, the self-diffusion of the mesogenic molecules computed in this work is still about 1 order of magnitude slower than that of simple liquids (see also Figure S9), which is consistent with the long time required for the spontaneous transition. The latter can again be placed at ∼34.5 °C, based on the different behavior of the diffusion coefficients computed in the nematic and isotropic phases.

In fact, as evident from the top panel of Figure 4, in the nematic phase the diffusion coefficient along or perpendicular to the phase director $\hat{\mathbf{n}}$ takes significantly distinct values, where in the former direction the translation is even faster than the isotropic phase, whereas any displacement transverse to $\hat{\mathbf{n}}$ is disfavored.

Turning to the single-molecule rotation, as detailed in the Supporting Information, the rotational diffusion coefficients D^{rot}, connected to the molecular spinning (*i.e.*, the rotation of the molecule around its long molecular axis) and tumbling (*i.e.*, the rotation of the long axis itself) motions, can be computed by integrating the correlation function of the molecular angular velocity. As shown in Figure S10, molecular spinning and tumbling take place on a much smaller time scale (∼10 ps) with respect to translation, with the former motion being 1 order of magnitude faster than the latter. Yet, as displayed in the middle panel of Figure 4, the agreement with the available experimental data[45] is very good, validating the MD description also on fast time scales. It should be noted that the tumbling coefficient D^{rot}_{tumb} is known to suffer of a certain degree of experimental indeterminacy,[64] and it is often assumed to be biased by some model approximation.[45] In this framework, the possibility of accurately predicting this value *in silico* also allows for reliable estimates, *i.e.*, supported by the validation against experiment of a large variety of other molecular and macroscopic properties, of other LC key features, as for instance the rotational viscosity, γ_1, an observable directly related to the response time of LC-based devices.[65]

In fact, as detailed in eq S18, γ_1 can be obtained according to the Fialkowski approach[66] from the sole knowledge of the second- and fourth-order parameters and the tumbling diffusion coefficient. The excellent agreement with the experimental measures, evidenced in Table 4 for the value computed at room temperature, appears also in the bottom panel of Figure 4, where the temperature dependence of the computed and experimental[43] γ_1 is displayed. In Table 4 are also reported the activation energies of all the investigated dynamic properties, obtained by fitting the temperature dependence of the proper quantity, according to the Arrhenius law reported in eqs S16, S17, and S19. The global agreement resulting with respect to the experimental activation energies further confirms the validity of the MD description both across several time scales and in different thermodynamic (temperature) conditions.

In conclusion, we have shown that by using an "*ab initio*" based approach we can obtain a truly multiscale description of complex self-assembly processes, as for instance the temperature-driven reorganization of an isotropic liquid to an orientationally ordered nematic phase. Concretely, the results obtained with MD runs employing an accurate QMD-FF, specifically tailored for the 5CB nematogen,[31] were found in a noticeable quantitative agreement with a *plethora* of experiments characterizing different stages of this process. Furthermore, the MD capability to bridge several time scales,

https://doi.org/10.1021/acs.jpclett.1c03517
J. Phys. Chem. Lett. XXXX, XXX, XXX−XXX

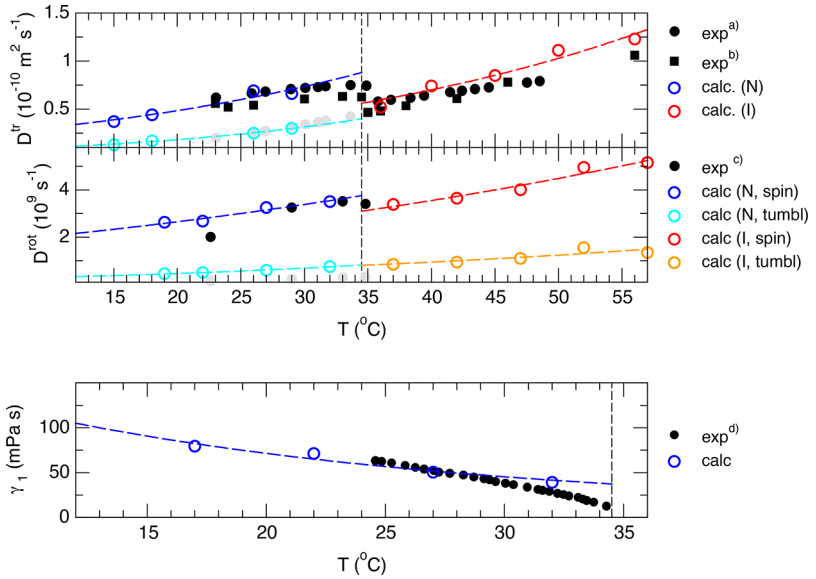

Figure 4. Dynamic properties obtained for the MD production runs at 1 atm in the 17−57 °C range. Top panel: experimental (full symbols) and computed (empty circles) translational diffusion coefficients D^{tr}, in the nematic (N) and isotropic (I) phase. Dark and bright colors correspond to the diffusion along and transverse to the phase director, respectively. Middle panel: experimental (full circles) and computed (empty circles) rotational diffusion coefficients D^{rot}, in the nematic (N) and isotropic (I) phase. Dark and bright colors correspond to the spinning and tumbling motions, respectively. The latter are enhanced by a factor of 5 for visualization purposes. Bottom panel: experimental (full circles) and computed (empty circles) rotational viscosity (γ_1). In all panels, dashed lines show the resulting Arrhenius fit. (a) Ref 50, (b) ref 54, (c) ref 45, and (d) ref 43.

Table 4. Computed and Experimental Dynamic Properties of the LC Material

property	this work	exp. [ref]
γ_1 (mPa s, 27 °C)	50.9	38.8−52.6 [43, 56]
ΔE^{tr}_{iso} (kJ/mol)	32 ± 1	32.8 ± 0.5 [50]
$\Delta E^{tr}_{\parallel}$ (kJ/mol)	30 ± 2	25 ± 2.5 [50]
$\Delta E^{tr}_{\perp}$ (kJ/mol)	40 ± 2	39 ± 2.5 [50]
ΔE^{rot}_{spin} (kJ/mol)	17.9 ± 0.3	13.5 [45]
ΔE^{rot}_{tum} (kJ/mol)	29.5 ± 0.3	33.5 [45]
$\Delta E^{\gamma 1}$ (kJ/mol)	33.5	32.5 [44, 56]

of utmost relevance yet often absent in experimental ensemble averages, was exploited to gain a picosecond detailed atomic understanding of the self-assembly processes and associated instabilities, which is corroborated by the reliability of the description achieved for the slow collective reorientation. For instance, the possibility to accurately estimate quantities like the rotational diffusion coefficient, connected to the single-molecule tumbling motion and hardly obtainable with experimental techniques, allows for a reliable prediction of key material properties as the rotational viscosity. Moreover, the possibility to dissect the slow collective reorientation on a picosecond scale and the atomistic view achievable for single molecular events as conformational changes have allowed for a deeper insight into the self-assembly mechanics. The present results in fact suggest that the slow transition toward the ordered nematic phase takes place in a two-step process: the alignment of the biphenyl *p*-axis of two neighboring molecules is first accompanied by an elongation of the aliphatic chains (which are rearranged in the more extended all-*trans* conformation) and then proceeds without significant variation in the conformer population. The remarkable accuracy, achieved on a wide range of structural and dynamical properties at varied thermodynamic conditions, and the intrinsic, first-principles-based predictive capability of the FF, indeed the two most desired attributes for *in silico* design, confirm the crucial role that QMD-FF-based approaches could play in a truly bottom-up engineering of advanced materials. Finally, it might be worth mentioning that, although QMD-FFs were designed to exploit system specificity to enhance the achievable accuracy, it would be interesting to test to what degree and with what effort they could be transferred to similar mesogenic systems. However, considering the computational cost connected with the extended MD runs carried out in the present work, such testing is outside the scope of the present Letter, and it will be the object of future work.

■ ASSOCIATED CONTENT

Supporting Information

The Supporting Information is available free of charge at https://pubs.acs.org/doi/10.1021/acs.jpclett.1c03517.

Additional details on QMD-FF and MD simulations; calculations of the orientational, thermodynamic and diffusion properties; additional figures on the reorganization dynamics (PDF)

■ AUTHOR INFORMATION

Corresponding Author

Giacomo Prampolini − *Istituto di Chimica dei Composti OrganoMetallici (ICCOM-CNR), I-56124 Pisa, Italy;* orcid.org/0000-0002-0547-8893; Email: giacomo.prampolini@pi.iccom.cnr.it

Authors

Leandro Greff da Silveira − *Instituto de Química, Universidade Federal do Rio Grande do Sul, 91 501-970 Porto Alegre, Brazil*

J. G. Vilhena − *Department of Physics, University of Basel, 4056 Basel, Switzerland;* orcid.org/0000-0001-8338-9119

https://doi.org/10.1021/acs.jpclett.1c03517
J. Phys. Chem. Lett. XXXX, XXX, XXX−XXX

Paolo Roberto Livotto − *Instituto de Química, Universidade Federal do Rio Grande do Sul, 91 501-970 Porto Alegre, Brazil*

Complete contact information is available at: https://pubs.acs.org/10.1021/acs.jpclett.1c03517

Notes

The authors declare no competing financial interest.

■ ACKNOWLEDGMENTS

Prof. Ivo Cacelli is gratefully acknowledged for the many useful discussions and for his inspiring ideas. G.P. acknowledges Dr. Fabrizio Santoro for nice suggestions and a careful reading of the manuscript. J.G.V. acknowledges funding from a Marie Sklodowska-Curie Fellowship within the Horizon 2020 framework (Grant Number DLV-795 286) and the Swiss National Science Foundation (Grant Number CRSK-2 190 731/1). The authors thankfully acknowledge the computer resources, technical expertise, and assistance provided by the Red Española de Supercomputación (RES) at the Minotauro and CTE-Power9 supercomputers (BSC, Barcelona).

■ REFERENCES

(1) Heckl, W. M. *Molecular Self-Assembly and the Origin of Life In Astrobiology: The Quest for the Conditions of Life*; Horneck, G., Baumstark-Khan, C., Eds.; Springer: Berlin, 2002; pp 361−372.

(2) Lee, Y. S. *Self-Assembly and Nanotechnology*; John Wiley & Sons, Inc.: Hoboken, NJ, 2008.

(3) Stupp, S. I.; Palmer, L. C. Supramolecular Chemistry and Self-Assembly in Organic Materials Design. *Chem. Mater.* **2014**, *26*, 507−518.

(4) Mali, K. S.; Pearce, N.; De Feyter, S.; Champness, N. R. Frontiers of supramolecular chemistry at solid surfaces. *Chem. Soc. Rev.* **2017**, *46*, 2520−2542.

(5) Wang, H.; Feng, Z.; Xu, B. Bioinspired assembly of small molecules in cell milieu. *Chem. Soc. Rev.* **2017**, *46*, 2421−2436.

(6) Azevedo, H. S.; da Silva, R. M. P. *Self-assembling Biomaterials*; Woodhead Publishing Series in Biomaterials; Woodhead Publishing, 2018.

(7) Huang, Z.; Song, W.; Chen, X. Supramolecular Self-Assembled Nanostructures for Cancer Immunotherapy. *Front. Chem.* **2020**, *8*, 380.

(8) Palma, C. A.; Cecchini, M.; Samorí, P. Predicting self-assembly: From empirism to determinism. *Chem. Soc. Rev.* **2012**, *41*, 3713−3730.

(9) Mendes, A. C.; Baran, E. T.; Reis, R. L.; Azevedo, H. S. Self-assembly in nature: Using the principles of nature to create complex nanobiomaterials. *Wiley Interdisciplinary Reviews: Nanomedicine and Nanobiotechnology* **2013**, *5*, 582−612.

(10) Frederix, P. W.; Patmanidis, I.; Marrink, S. J. Molecular simulations of self-assembling bio-inspired supramolecular systems and their connection to experiments. *Chem. Soc. Rev.* **2018**, *47*, 3470−3489.

(11) Tschierske, C. Liquid Crystals: Materials Design and Self-assembly. *Topics in Current Chemistry* **2011**, *318*, 1.

(12) Lu, Z.; Godfrey, H. G. W.; da Silva, I.; Cheng, Y.; Savage, M.; Tuna, F.; McInnes, E. J. L.; Teat, S. J.; Gagnon, K. J.; Frogley, M. D.; et al. Modulating supramolecular binding of carbon dioxide in a redox-active porous metal-organic framework. *Nat. Commu* **2017**, *8*, 14212.

(13) Nickmans, K.; Schenning, A. P. H. J. Directed Self-Assembly of Liquid-Crystalline Molecular Building Blocks for Sub-5 nm Nano-patterning. *Adv. Mater.* **2018**, *30*, 1703713.

(14) Kassem, S.; Van Leeuwen, T.; Lubbe, A. S.; Wilson, M. R.; Feringa, B. L.; Leigh, D. A. Artificial molecular motors. *Chem. Soc. Rev.* **2017**, *46*, 2592−2621.

(15) Bishop, K. J. M.; Wilmer, C. E.; Soh, S.; Grzybowski, B. A. Nanoscale Forces and Their Uses in Self-Assembly. *Small* **2009**, *5*, 1600.

(16) Adler-Abramovich, L.; Gazit, E. The physical properties of supramolecular peptide assemblies: from building block association to technological applications. *Chem. Soc. Rev.* **2014**, *43*, 6881−6893.

(17) Kolesnichenko, I. V.; Anslyn, E. V. Practical applications of supramolecular chemistry. *Chem. Soc. Rev.* **2017**, *46*, 2385−2390.

(18) Orsi, M. *Molecular simulation of self-assembly In Self-assembling Biomaterials*; Azevedo, H. S., da Silva, R. M., Eds.; Woodhead Publishing, 2018; pp 305−318.

(19) Frenkel, D.; Smith, B. *Understanding Molecular Simulations*; Academic Press: San Diego, 1996.

(20) Pal, S.; Ray, B. C. *Molecular Dynamics Simulation of Nanostructured Materials*; CRC Press, 2020.

(21) Allen, M. P.; Tildesley, D. J. *Computer Simulation of Liquids*; Clarendon: Oxford, 1987.

(22) Bonomi, M.; Camilloni, C. *Biomolecular Simulations*; Methods Mol. Biol., Vol. *2022*; Springer: New York, 2019.

(23) Wildman, J.; Repiščák, P.; Paterson, M. J.; Galbraith, I. General Force-Field Parametrization Scheme for Molecular Dynamics Simulations of Conjugated Materials in Solution. *J. Chem. Theory Comput.* **2016**, *12*, 3813−3824.

(24) Silva, G. M. C.; Morgado, P.; Lourenço, P.; Goldmann, M.; Filipe, E. J. M. Spontaneous self-assembly and structure of perfluoroalkylalkane surfactant hemimicelles by molecular dynamics simulations. *Proc. Natl. Acad. Sci. U. S. A.* **2019**, *116*, 14868−14873.

(25) Jiang, L.; Rogers, D. M.; Hirst, J. D.; Do, H. Force Fields for Macromolecular Assemblies Containing Diketopyrrolopyrrole and Thiophene. *J. Chem. Theory Comput.* **2020**, *16*, 5150−5162.

(26) Boyd, N. J.; Wilson, M. R. Validating an optimized GAFF force field for liquid crystals: T NI predictions for bent-core mesogens and the first atomistic predictions of a dark conglomerate phase. *Phys. Chem. Chem. Phys.* **2018**, *20*, 1485−1496.

(27) Allen, M. P. Molecular simulation of liquid crystals. *Mol. Phys.* **2019**, *117*, 2391.

(28) König, G.; Riniker, S. On the faithfulness of molecular mechanics representations of proteins towards quantum-mechanical energy surfaces. *Interface Focus* **2020**, *10*, 20190121.

(29) Spicher, S.; Grimme, S. Robust Atomistic Modeling of Materials, Organometallic, and Biochemical Systems. *Angew. Chem., Int. Ed.* **2020**, *59*, 15665−15673.

(30) Odinokov, A.; Yakubovich, A.; Son, W.-j.; Jung, Y.; Choi, H. Exploiting the quantum mechanically derived force field for functional materials simulations. *Comput. Mat* **2021**, *7*, 155.

(31) Vilhena, J. G.; Greff da Silveira, L.; Livotto, P. R.; Cacelli, I.; Prampolini, G. Automated Parameterization of Quantum Mechanically Derived Force Fields for Soft Materials and Complex Fluids: Development and Validation. *J. Chem. Theory Comput.* **2021**, *17*, 4449−4464.

(32) Cacelli, I.; Prampolini, G. Parametrization and Validation of Intramolecular Force Fields Derived from DFT Calculations. *J. Chem. Theory Comput.* **2007**, *3*, 1803−1817.

(33) Cerezo, J.; Prampolini, G.; Cacelli, I. Developing accurate intramolecular force fields for conjugated systems through explicit coupling terms. *Theor. Chem. Acc.* **2018**, *137*, 80.

(34) Cacelli, I.; Cimoli, A.; Livotto, P. R.; Prampolini, G. An Automated Approach for the Parameterization of Accurate Intermolecular Force-Fields: Pyridine as a Case Study. *J. Comput. Chem.* **2012**, *33*, 1055.

(35) Prampolini, G.; Livotto, P. R.; Cacelli, I. Accuracy of Quantum Mechanically Derived Force-Fields Parameterized from Dispersion-Corrected DFT Data: The Benzene Dimer as a Prototype for Aromatic Interactions. *J. Chem. Theory Comput.* **2015**, *11*, 5182−96.

(36) Tiberio, G.; Muccioli, L.; Berardi, R.; Zannoni, C. Towards in Silico Liquid Crystals. Realistic Transition Temperatures and Physical Properties for n-Cyanobiphenyls via Molecular Dynamics Simulations. *ChemPhysChem* **2009**, *10*, 125−136.

(37) deGennes, P. G.; Prost, J. *The Physics of Liquid Crystals*, 2nd ed.; Oxford University Press: Oxford, 1993.
(38) Högberg, D.; Soberats, B.; Yatagai, R.; Uchida, S.; Yoshio, M.; Kloo, L.; Segawa, H.; Kato, T. Liquid-Crystalline Dye-Sensitized Solar Cells: Design of Two-Dimensional Molecular Assemblies for Efficient Ion Transport and Thermal Stability. *Chem. Mater.* **2016**, *28*, 6493−6500.
(39) Xie, Y.; Li, Y.; Wei, G.; Liu, Q.; Mundoor, H.; Chen, Z.; Smalyukh, I. I. Liquid crystal self-assembly of upconversion nanorods enriched by depletion forces for mesostructured material preparation. *Nanoscale* **2018**, *10*, 4218−4227.
(40) Park, W.; Ha, T.; Kim, T.-T.; Zep, A.; Ahn, H.; Shin, T. J.; Sim, K. I.; Jung, T. S.; Kim, J. H.; Pociecha, D.; et al. Directed self-assembly of a helical nanofilament liquid crystal phase for use as structural color reflectors. *NPG Asia Materials* **2019**, *11*, 45.
(41) Solodkov, N. V.; Shim, J.-u.; Jones, J. C. Self-assembly of fractal liquid crystal colloids. *Nat. Commun.* **2019**, *10*, 198.
(42) Emsley, J. W.; Luckhurst, G. R.; Stockley, C. P. A Theory of Orientational Ordering in Uniaxial Liquid Crystals Composed of Molecules with Alkyl Chains. *Proc. R. Soc. London A* **1982**, *381*, 117−138.
(43) Siedler, L. T. S.; Hyde, A. J.; Pethrick, R. A.; Leslie, F. M. Zvetkow Twist Viscosity Measurements of Some Nematic Liquid Crystals. *Mol. Cryst. Liq. Cryst.* **1983**, *90*, 255−270.
(44) Bock, F. J.; Kneppe, H.; Schneider, F. Rotational viscosity of nematic liquid crystals and their shear viscosity under flow alignment. *Liq. Cryst.* **1986**, *1*, 239−251.
(45) Dong, R. Y. Modeling of dynamics in liquid crystals from deuterium NMR. *J. Chem. Phys.* **1988**, *88*, 3962−3969.
(46) Magnuson, M. L.; Fung, B. M.; Bayle, J. P. On the temperature dependence of the order parameter of liquid crystals over a wide nematic range. *Liq. Cryst.* **1995**, *19*, 823−832.
(47) Sandmann, M.; Hamann, F.; Wurflinger, A. PVT Measurements on 4-n-Pentyl-4′-Cyano-Biphenyl (5CB) and trans-4-(4′-Octyl-Cyclohexyl)-Benzonitrile (8PCH) up to 300 MPa. *Z. Naturforsch., A: Phys. Sci.* **1997**, *52*, 739.
(48) Adam, C. J.; Ferrarini, A.; Wilson, M. R.; Ackland, G. J.; Crain, J. A first principles and mean field investigation of the conformational properties of 5CB. *Mol. Phys.* **1999**, *97*, 541−550.
(49) Oweimreen, G.; Morsy, M. DSC studies on p-(n-alkyl)-p′-cyanobiphenyl (RCB's) and p-(n-alkoxy)-p′-cyanobiphenyl (ROCB's) liquid crystals. *Thermochim. Acta* **2000**, *346*, 37−47.
(50) Dvinskikh, S. V.; Furó, I. Anisotropic self-diffusion in the nematic phase of a thermotropic liquid crystal by 1H-spin-echo nuclear magnetic resonance. *J. Chem. Phys.* **2001**, *115*, 1946−1950.
(51) Roushdy, M. Optical Behavior and Related Properties of the Binary Mixture 5CB/8CB Liquid Crystals. *Mol. Cryst. Liq. Cryst.* **2006**, *457*, 151−160.
(52) Emsley, J. W.; Lesot, P.; De Luca, G.; Lesage, A.; Merlet, D.; Pileio, G. A comparison of proton-detected ^{13}C local field experiments with deuterium NMR at natural abundance for studying liquid crystals. *Liq. Cryst.* **2008**, *35*, 443−464.
(53) Deschamps, J.; Trusler, J. P.; Jackson, G. Vapor pressure and density of thermotropic liquid crystals: MBBA, 5CB, and novel fluorinated mesogens. *J. Phys. Chem. B* **2008**, *112*, 3918−3926.
(54) Cifelli, M.; De Gaetani, L.; Prampolini, G.; Tani, A. Atomistic Computer Simulation and Experimental Study on the Dynamics of the n Cyanobiphenyls Mesogenic Series. *J. Phys. Chem. B* **2008**, *112*, 9777−9786.
(55) Zgura, I.; Moldovan, R.; Beica, T.; Frunza, S. Temperature dependence of the density of some liquid crystals in the alkyl cyanobiphenyl series. *Cryst. Res. Technol.* **2009**, *44*, 883−888.
(56) Orr, R.; Pethrick, R. A. Viscosity coefficients of nematic liquid crystals: I. Oscillating plate viscometer measurements and rotational viscosity measurements: K15†. *Liq. Cryst.* **2011**, *38*, 1169−1181.
(57) Javadian, S.; Dalir, N.; Gilani, A. G.; Kakemam, J.; Yousefi, A. A new approach to study interaction parameters in cyanobiphenyl liquid crystal binary systems. *J. Chem. Thermodyn.* **2015**, *80*, 22−29.
(58) Bezrodna, T.; Klishevich, G.; Melnyk, V.; Nesprava, V.; Roshchin, O.; Drozd, M. Low-temperature luminescence and phase structure of 5CB liquid crystal under different cooling regimes. *Mol. Cryst. Liq. Cryst.* **2018**, *672*, 159−167.
(59) Abraham, M. J.; Murtola, T.; Schulz, R.; Páll, S.; Smith, J. C.; Hess, B.; Lindahl, E. GROMACS: High performance molecular simulations through multi-level parallelism from laptops to supercomputers. *SoftwareX* **2015**, *1−2*, 19−25.
(60) Cacelli, I.; Prampolini, G.; Tani, A. Atomistic Simulation of a Nematogen Using a Force Field Derived from Quantum Chemical Calculations. *J. Phys. Chem. B* **2005**, *109*, 3531−3538.
(61) Gaetani, L. D.; Prampolini, G.; Tani, A. Modeling a Liquid Crystal Dynamics by Atomistic Simulation with an Ab Initio Derived Force Field. *J. Phys. Chem. B* **2006**, *110*, 2847−2854.
(62) Cacelli, I.; De Gaetani, L.; Prampolini, G.; Tani, A. Liquid Crystal Properties of the n-Alkyl-cyanobiphenyl Series from Atomistic Simulations with Ab Initio Derived Force Fields. *J. Phys. Chem. B* **2007**, *111*, 2130−2137.
(63) Cacelli, I.; Cimoli, A.; De Gaetani, L.; Prampolini, G.; Tani, A. Chemical Detail Force Fields for Mesogenic Molecules. *J. Chem. Theory Comput.* **2009**, *5*, 1865−1876.
(64) Calucci, L.; Geppi, M. CAGE: Software for a Critical Analysis of ^{2}H Spin-Lattice Relaxation in Liquid Crystals. *J. Chem. Inf. Comput. Sci.* **2001**, *41*, 1006−1014.
(65) Wang, L.; Sun, J.; Liu, H.; Chigrinov, V. G.; Kwok, H. S. Increasing the rewriting speed of ORW e-paper by electric field. *Liq. Cryst.* **2018**, *45*, 553−560.
(66) Fiałkowski, M. Viscous properties of nematic liquid crystals composed of biaxial molecules. *Phys. Rev. E: Stat. Phys., Plasmas, Fluids, Relat. Interdiscip. Top.* **1998**, *58*, 1955−1966.

https://doi.org/10.1021/acs.jpclett.1c03517
J. Phys. Chem. Lett. XXXX, XXX, XXX−XXX